Theory of Force Transducer Design Optimization for Die Wall Stress Measurement During Tablet Compaction: Optimization and Validation of Split-Web Die Using Finite Element Analysis

Chuntien Yeh,[1] Syed A. Altaf,[2] and Stephen W. Hoag[3,4]

Received May 12, 1997; accepted June 11, 1997

Purpose. 1) To illustrate how computer aided engineering stress analysis can be used to improve the transducer design process for tablet press instrumentation; 2) to use these optimal design procedures for the geometric optimization of a cylindrical, segmented, and a novel split-web die design. Discussion includes the selection of optimal die wall thickness, segment cutting angle, strain gage placement, Wheatstone bridge configuration, and the influence of tablet height and position within the die on signal output.

Methods. Stress analysis was done with a finite element analysis (FEA) software package running on a personal computer.

Results. For the segmented die, the admissible range of die wall thicknesses depends upon cutting angle; the signal output is non-linear because the stress distribution in the die wall is influenced by tablet height and position within the die. For the split-web die, the optimal configuration consists of a 1/8 in. sensing web with a strain gage located at the peak of the sensing-web arch. This prototype had a linear calibration curve ($r^2 = 0.999$) with no hysteresis. Radial versus axial stress transmission curves for: starch and sodium chloride were consistent with literature data.

Conclusions. Finite element analysis (FEA) is a useful numerical tool for the systematic optimization of tablet press instrumentation. By enclosing the sensing web of a three layered die design in a cylinder, the split-web design can be directly mounted without modification of the die table.

KEY WORDS: force transducer design and design optimization; split-web die; design-by-analysis approach; finite element analysis (FEA); die wall stress measurement; tablet compaction.

[1] Freightliner Co., 4747 N Channel Ave., PO Box 3849, Portland, Oregon 97208.

[2] Cibus Pharmaceutical Inc. 887 Mitten Rd., Burlingame, California 94010.

[3] School of Pharmacy, University of Maryland at Baltimore, 20 N Pine Street, Baltimore, Maryland 21201.

[4] To whom correspondence should be addressed. (e-mail: shoag@umabnet.ab.umd.edu)

ABBREVIATIONS: DWS, Die-wall stress; E, Young's modulus; *GF*, Gage factor; h, Height of die; p_i, Pressure at inner die wall; P_g, Maximum power dissipation; P_{max}, Maximum compaction pressure; *r*, Radial location $r_i \leq r \leq r_e$; r_e, Radius of external surface; r_i, Bore radius of die; R_g, Gage resistance; *SF*, Safety factor; *t*, Die wall thickness; V_i, Wheatstone bridge input voltage; V_o, Wheatstone bridge output voltage; ε_a, Axial strain; ε_θ, Tangential strain; β, r_e/r; λ, r_e/r_i; ρ, R_2/R_1; ϕ, Cutting angle; includes angle on sensing web; υ, Poisson's ratio; $\sigma_{1,2,3}$, Principal stresses; σ_{vm}, Von Mises stress; σ_{app}, Equivalent applied stress; σ_{yd}, Yield strength.

INTRODUCTION

Because it is the design geometry and associated strain gage arrangement which determines the performance characteristics of a transducer, there have been many different designs and special gage configurations developed for the optimization of die-wall stress (DWS) measurement (1–6). Of all these designs, the segmented die has become the most popular, Figure 1a. When designing a transducer for die-wall stress measurement, two major concerns are the effects of tablet height and tablet position within the die on output signal. These two factors can make calibration and data interpretation more difficult because they interact, causing the transducer to have a non-linear output signal. To address these concerns, the segmented die design has been modified over time to achieve better signal output (7–9).

A different approach for improving DWS measurement is the three-layered die developed by Rippie and Danielson (6). By integrating a sensing web into a thin middle layer, this design isolates stress measurement to a narrow band around the tablet, which gives a much closer approximation to the true stress. In addition, because the stress/strain distribution in the sensing web is completely uncoupled from all other die wall stresses and strains, DWS measurement is linear and independent of tablet height and position within the die (as long as the sensing web has full contact with the tablet). Thus, changes in DWS with tablet height can be accounted for. The reason for the linear response can best be understood by considering Lame's

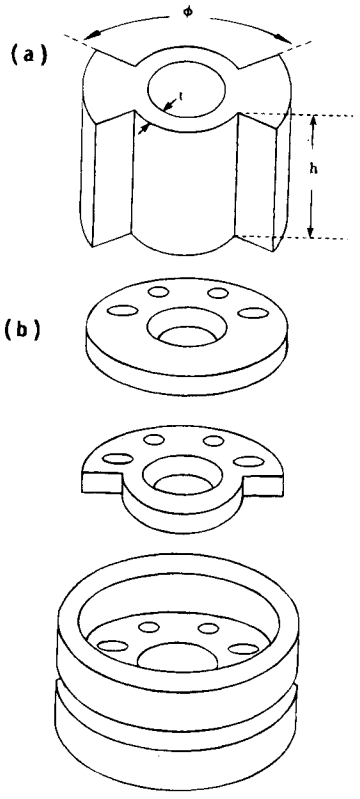

Fig. 1. The symmetric segmented die; ϕ: cut-away angle, *t*: effective wall thickness and h: die height (a). Assembly of the three layer split web die design (b).

0724-8741/97/0900-1161$12.50/0

solution (10) for the stress/strain distribution in a hollow cylinder, which predicts that the tangential strain on the outer die surface is a linear function of a uniformly applied internal pressure. Even though the boundary conditions of the sensing web don't completely match Lame's this linear relationship still holds, see Saint-Venant's principle (10). A disadvantage of Rippie's design is that the die table must be significantly modified to accommodate transducer mounting, because the standard horizontal die lock-screw causes the layers to tilt, which binds the sensing web.

To avoid modifying the die table, the authors propose a split-web die concept which encloses the sensing web in a cylinder, thereby avoiding sensing web binding, see Figure 1b. To obtain the best design, the sensing web configuration must be optimized. The primary design variables to be optimized are the sensing web thickness and the strain gage position on the sensing web.

Traditionally, transducer designs have resulted from a great deal of experimental trial-and-error. The current trial-and-error design process can be divided into four distinct phases: concept development, shape and material selection, prototype building, and prototype testing. In this process, a prototype is built and tested. If it doesn't deliver the desired performance, the design is modified and the cycle of prototype building and testing is repeated until the design has the desired performance characteristics. Drawbacks of this traditional design process are the time and expense associated with prototype building and physical testing.

To overcome the limitations of the trial-and-error method, this research will use an optimal design process (ODP), which is based upon a design-by-analysis approach. The difference between the trial-and-error method and the ODP is that, instead of building and testing a prototype, engineering-stress analysis is used to numerically simulate the performance characteristics of a transducer design. With this information the initial design decisions can be made without building a prototype; therefore, the complete design cycle can be done with fewer prototypes and a wider range of test conditions. As a result, important design constraints such as material failure, strain gage failure, and bridge output signal level can be simultaneously studied and optimized, ensuring the best performance possible from a particular design concept.

Except for the simplest geometries, this design-by-analysis approach is not practical without the use of high-performance computers. However, the commercialization of low-cost user-friendly software and the availability of high-performance personal computers makes the ODP much more feasible. At present, tablet press instrumentation is primarily designed by trial-and-error, but with all of these recent advances the authors feel that the design-by-analysis approach is now feasible for pharmaceutical researchers and merits further investigation.

Consequently, the goals of this paper are 1) to show how the design-by-analysis approach can be used to improve a transducer design and 2) to use this ODP to optimize our split-web design concept. To illustrate how engineering stress analysis can be adapted to the design of tablet press instrumentation the discussion will begin with: 1) the general principles needed for a design-by-analysis approach; 2) then the geometric optimization of a cylindrical and symmetrically segmented die will be performed. 3) Finally, the optimal design process will be used to optimize the authors' split-web design concept. To confirm the effectiveness and signal linearity of the transducer designed by the ODP a prototype was built and tested.

OPTIMAL DESIGN CONSTRAINTS AND METHODOLOGY

For a transducer to have a measurable signal the strain at the gage site must exceed the minimum detection limit of the strain gage and data acquisition system. Because reducing the die wall thickness concentrates the forces into a smaller area which increases the strain (at the gage site) and hence the signal output, the die wall must be thin enough so that the forces generated during compaction produce a measurable strain. Yet, the die wall must be thick enough to withstand the forces generated during compaction without yielding or rupturing. Thus, an optimally designed transducer must balance these competing demands of signal output and material failure.

Analysis of Material Failure

There are an infinite number of combinations for the multiaxial loading of a material that can lead to its failure. Because it is impossible to characterize all of these combinations, failure criteria have been developed which use the uniaxial tensile strength to predict when multiaxial failure will occur. There are many accepted methods, such as the maximum normal stress, maximum shear stress and Von Mises stress (distortion energy theory) criteria. Collins (11) provides a comprehensive review of these methods. Generally, failure criteria give rules for the calculation of a single equivalent applied stress (σ_{app}), from the multiaxial loading conditions, which can be compared to the uniaxial yield strength. Thus, to avoid failure within any part of the transducer, the σ_{app} must not exceed the uniaxial yield strength (σ_{yd}) of the transducer material.

$$\sigma_{app} \leq \sigma_{yd} \tag{1}$$

In this paper, the equivalent applied stress is defined by the distortional energy theory, or Von Mises stress (σ_{vm}), which can be expressed as

$$\sigma_{vm} = \sqrt{\frac{1}{2}[(\sigma_1 - \sigma_2)^2 + (\sigma_2 - \sigma_3)^2 + (\sigma_3 - \sigma_1)^2]} \tag{2}$$

where σ_1, σ_2, and σ_3 are the principal stresses (11).

To reduce the chances of catastrophic material failure brought about by uncertainties in material strength and in the loads acting upon the die, a safety factor (SF) is inserted into the applied stress equation (12). Thus, the equivalent applied stress (σ_{app}) defined by the Von Mises criterion is written as

$$\sigma_{app} = SF \cdot \sigma_{vm} = SF \cdot \sqrt{\frac{1}{2}[(\sigma_1 - \sigma_2)^2 + (\sigma_2 - \sigma_3)^2 + (\sigma_3 - \sigma_1)^2]} \tag{3}$$

Output Signal Measurement Limitations

Typically, detection of stress is accomplished by bonded electrical-resistance strain gages configured in a Wheatstone bridge. The output voltage (V_o) from a Wheatstone bridge is usually in the millivolt range. With such low level signals, obtaining a satisfactory signal-to-noise ratio is difficult, espe-

cially with the electrical noise in the measurement environment. When designing a transducer particular attention must be paid to the relationship between signal output and strain at the gage site.

When electrical-resistance strain gages are strained, their resistance changes; the equation governing this change is (13)

$$\frac{\Delta R}{R} = GF\varepsilon_a \tag{4}$$

where ΔR is the change in resistance R, and ε_a is the axial strain. The gage factor (GF) is the proportionality constant between the axial strain and the change in resistance. For strains less than 10,000 $\mu\varepsilon$ the equation governing the output of the Wheatstone bridge is

$$V_o = V_i \frac{\rho}{(1+\rho)^2}\left(\frac{\Delta R_1}{R_1} - \frac{\Delta R_2}{R_2} + \frac{\Delta R_3}{R_3} - \frac{\Delta R_4}{R_4}\right) \tag{5}$$

where V_i is the bridge excitation voltage, R_1, R_2, R_3, and R_4 are the resistances of the bridge arms, and ρ is the ratio R_2/R_1 (13). By substituting Eqn. 4 into Eqn. 5, the general linear relationship for bridge output V_o and the surface strain ε_i at the different gage sites can now be expressed as:

$$V_o = S_r\varepsilon_{eff} \tag{6}$$

where S_r is the overall bridge sensitivity, and ε_{eff} is the effective strain for the bridge, which is expressed as:

$$\varepsilon_{eff} = \sum_{i=1}^{n} \varepsilon_i \tag{7}$$

where n is the number of active strain gages used to configure the bridge. Consequently, the bridge sensitivity, which depends on bridge configuration, can be expressed as:

$$S_r = V_i \frac{\rho}{(1+\rho)^2} nGF \tag{8}$$

Every data acquisition system has an optimal detection range with a lower limit (V_{min}). To acquire data the lower detection limit imposes the constraint, $V_o \geq V_{min}$, on bridge output; with the application of Eqn. 6, this inequality can be expressed in terms of the effective strain:

$$V_{min} \leq S_r\varepsilon_{eff} \tag{9}$$

Eqn. (9) summarizes the electronic constraints for transducer design, and along with Eqn. 8 they also illustrate three methods for improving output signal detection. First, V_{min} can be lowered by improving signal processing equipment. This method is independent of transducer design and beyond the scope of this paper. Second, the S_r can be increased either by increasing the number of active gages or the excitation voltage. Assuming no electronic cancellation or resistance, reconfiguring the bridge is limited to a four-fold increase. Secondly, the bridge excitation voltage can be increased. However, because excessive power dissipation in the gages will cause temperature changes that introduce errors in measurement (14), increases in the bridge excitation voltage are limited. The third way of increasing the output voltage is to increase the strain level at the gage site. With the segmented die, the strain is increased by decreasing the die wall thickness in the cut-away portion; however, the die wall cannot be made too thin because yielding and fracture may occur.

Strain Gage Limitations

The primary constraints imposed by a strain gage are the gage elongation and gage fatigue limits. All strain gages have elongation limits, that if exceeded, will permanently damage the strain gage. Typical elongation limits for a strain gage range from 0.5% to 5%, depending upon factors such as grid alloy, matrix construction, bonding adhesive and gage size (13). In addition, gages can also fail in fatigue because cyclic loading of a gage causes the grid alloy to work harden, resulting in a permanent resistance change. The fatigue life depends on the strain level. For example, the fatigue life of a Constantan strain gage increases from 10^2 cycles to greater than 10^8 cycles when the cyclic strain level drops from 2,700 $\mu\varepsilon$ to 1,200 $\mu\varepsilon$ (13). Because this fatigue strain limit (1,200 $\mu\varepsilon$) is more stringent it will be used as the strain gage elongation limit. Because the commonly used D3 tool steel is very brittle, the transducer will typically yield or fracture before the strain gage fails; thus, strain gage limits do not usually impose significant constraints on transducers constructed from brittle materials.

Finite Element Method

Finite element analysis is a numerical method for approximating the governing equations (stress/strain fields) of any continuous body. The first step in FEA is to generate a finite element model, which is a geometric representation of the actual mechanical component being analyzed. This model is created by dividing the actual component into a large number of subdivisions called, "finite elements." These elements are interconnected at specified points called "nodes" or "nodal points." The nodes lie on the element boundaries and are the points where adjacent elements are connected. To create a finite element mesh of a mechanical component, the user enters the geometric dimensions of the component into the FEA software. Once the geometric model has been created, the material properties, boundary conditions and loading conditions are then used to calculate the stress/strain fields. For more information on FEA the reader can refer to excellent texts, such as Cook *et al.* (15), Rao (16) and Champion (17).

EXPERIMENTAL

Design Examples

The following material properties, of a D3 tool steel, were used for all finite element analyses: Young's modulus 2×10^5 MPa, Poisson's ratio 0.3 and a yield strength 340 MPa. The following parameters, of a model EA-06-031DE-120, (Measurements Group, Inc., Raleigh, NC) strain gage, were used for all strain gage calculations: gage factor 2.01, maximum power dissipation 0.15 W and a gage resistance 120 Ω. All stress/strain calculations were done using the commercially available FEA program, COSMOS/M (Structural Research & Analysis Corp., Los Angeles, CA), running on a personal computer.

Press Instrumentation

A Stokes B2 rotary tablet press (F.J. Stokes Machine Company, Philadelphia, PA) equipped with 3/8 in. flat faced punches was used for tablet compaction. The ejection cam was removed to allow for residual die wall stress measurement. Lower punch

stress was measured with an instrumented compression roller pin (Specialty Measurements Inc., Pittstown, NJ). A bonded electrical resistant strain gage (EA-06-031DE-120, Micro-Measurements, Raleigh, NC) was placed on the sensing web at $\phi = 0°$ and configured into a single arm Wheatstone bridge. The electronic signals from the instrumented die, roller pin and proximity sensor were sent to a personal computer interfaced with a 12-bit 100 kHz analog to digital (A/D) converter (model AT-MIO-16, National Instruments Corp., Austin, TX).

Two different prototypes of the sensing web were built with a sensing web thickness of 1/8 in. or 1/16 in.. Both prototypes had: web height 1/8 in., inner bore diameter 3/8 in., outer diameter 7/8 in., alignment pin hole diameter 1/8 in. and screw hole diameter 5/32 in.. To allow free movement between the web and adjacent layers, the sensing web was made 1/10,000 in. thinner than the rest of the middle section. This clearance is small enough to prevent tableting material from extruding between adjacent layers. The die was calibrated in triplicate with Neoprene rubber plugs and an instrumented punch; the pressure was applied by filling the die with the rubber plugs and manually rotating the turret through the loading, dwell and unloading phases.

Tablet Compaction

Starch (Sta-Rx 1500, Colorcon, Westpoint, PA) and sodium chloride (Mallinckrodt AR, Paris, KY) were used for the compaction studies. For lubrication, a 20% slurry of magnesium stearate in isopropyl alcohol was swabbed onto the die wall and dried before compaction. The die was hand-filled and the tablets were compressed with an average turret angular velocity of $\omega = 4.62$ rads/sec. To maintain compression roller alignment and symmetry, the upper compression roller eccentric cam and the eye-bolt position were fixed; thus, the desired compaction pressure was achieved by varying the fill weight.

DESIGN EXAMPLES

Cylindrical Die Design

To illustrate the analytical method, the admissible range of die wall thicknesses will be calculated for a cylindrical die described by Watt (18). Although DWS depends on tablet height and location during compaction, these stress/strain calculations will be done assuming a uniform radial pressure (p_i) applied to the entire inner surface of the die. This assumption simulates the severest loading conditions. In addition, it will be assumed that only radial die wall forces are present and the ends of the die are free of any applied loads, these assumptions eliminate all axial stresses within and on the die wall. Even though punch movements during compaction generate die-wall friction, as shown in the literature for most lubricated formulations the axial forces generated by die-wall friction are small enough (19–21) to be neglected when calculating the Von Mises stress and tangential strain on the outer die wall.

The above conditions reduce the analysis to a two-dimensional plane strain problem, which makes the analytical solution more tractable. The problem of uniform pressure in a cylinder is called Lame's problem. The solutions for the radial (σ_r) and tangential (σ_θ) stresses are given by (10,22):

$$\sigma_r = -p_i \frac{\left[\left(\frac{r_e}{r}\right)^2 - 1\right]}{\lambda^2 - 1} \tag{10a}$$

and

$$\sigma_\theta = p_i \frac{\left[\left(\frac{r_e}{r}\right)^2 + 1\right]}{\lambda^2 - 1} \tag{10b}$$

where $\lambda = r_e/r_i = 1 + t/r_i$. In addition, the tangential strain is given by

$$\varepsilon_\theta = \frac{2r_i^2 p_i}{E(r_e^2 - r_i^2)} \tag{11}$$

where E is Young's elastic modulus.

Failure Analysis

Once the stress/strain fields have been determined, the minimal die wall thickness which does not yield can be calculated using the Von Mises failure criterion, Eqn. 2. The principal stresses are the three normal stresses that occur when the coordinate axes are aligned so that all shear stresses equal zero, and because there are no shear stresses for the above loading conditions, the principal stresses are equal to the normal stresses; $\sigma_1 = \sigma_r$, $\sigma_2 = \sigma_\theta$, and $\sigma_3 = \sigma_z$. By substituting the principal stress Eqns. 10a and 10b into Eqn. 2, the Von Mises stress σ_{vm} becomes

$$\sigma_{vm} = [\sigma_r^2 + \sigma_\theta^2 - \sigma_r\sigma_\theta]^{1/2} = p_i \frac{\sqrt{3\beta^4 + 1}}{\lambda^2 - 1} \tag{12}$$

where $\beta = r_e/r$. Eqn. 12 shows that the maximum and minimum Von Mises stresses always occur at the inner and outer die wall surfaces, respectively, and as the die wall thickness increases the maximum Von Mises stress decreases.

To determine the minimum die wall thickness, the failure criterion is applied at the inner die wall surface, which is the critical point most likely to fail. The equivalent applied stress σ_{app} can be obtained by substituting Eqn. 12 into Eqn. 3 and noting that $\lambda = \beta$ when $r = r_i$:

$$\sigma_{yd} = SF \cdot p_i \frac{\sqrt{3\lambda^4 + 1}}{\lambda^2 - 1} \tag{13}$$

To calculate λ, the four roots of Eqn. 13 can be determined by twice applying the quadratic equation, with $p_i = 120$ MPa, $r_i = 5$ mm and $SF = 1.1$. Thus, for a cylindrical die the minimum die thickness required to prevent material yielding is

$$t \geq 3.89 \text{ mm}$$

Signal Output

These calculations are done for a cylindrical die with a single strain gage mounted horizontally on the outer surface of the die and with the gage configured into a non-temperature compensating, single arm Wheatstone bridge. To use Eqn. 9, the bridge sensitivity (S_r) must be calculated for a given bridge configuration and gage type. For a single active gage mounted

horizontally, the effective strain equals the tangential strain, $\varepsilon_{eff} = \varepsilon_\theta$, which can be calculated by Eqn. 11.

To obtain the maximum bridge sensitivity, Eqn. 8 must be expressed in terms of the maximum power dissipation, which does not induce temperature changes within the gage. To do this, the excitation voltage in Eqn. 8 must be expressed in terms of a gage's maximum power dissipation capability (P_g) and resistance (R_g). For a single arm bridge, V_i can be written as:

$$V_i = (1 + \rho)\sqrt{P_g R_g} \tag{14}$$

Substituting Eqn. 14 into Eqn. 8 and 9 yields for a single arm bridge:

$$S_R = \frac{V_o}{\varepsilon_{eff}} = \frac{\rho}{1 + \rho} GF\sqrt{P_g R_g} \tag{15}$$

To determine the maximum die wall thickness, first the minimum detectable strain at the gage site is calculated using Eqn. 15 and the lower detection limit V_{min}. Then the outer radius r_e can be calculated by substituting the minimum detectable strain into Eqn. 11 yielding:

$$\frac{2r_i^2 p_i}{E(r_e^2 - r_i^2)} \geq \varepsilon_{eff} = \frac{V_{min}}{S_r} \tag{16}$$

Thus, for $r_i = 5$ mm and $V_{min} = 0.5$ mV the admissible range of die-wall thicknesses at 120 MPa of die-wall compact pressure are:

$$0 < t \leq 11.76\ mm$$

Strain Gage Limitations

By substituting $\varepsilon_{fatigue}$ for ε_{eff}, Eqn. 16 can be used to calculate the minimum die wall thickness needed to prevent strain gage damage. As discussed above, the strain gage fatigue limit of 1200 $\mu\varepsilon$ is used for the maximum strain gage elongation. With this constraint, the minimum wall thickness required to prevent damage to the installed strain gages at a P_{max} of 120 MPa is 2.09 mm. Because the gage limit is larger than the failure limit, constraints imposed by the strain gages are not important in this situation.

Summary

In conclusion, the die-wall thicknesses which produce a measurable bridge output signal without damaging the transducer or the installed strain gages are

$$3.98\ mm \leq t \leq 11.76\ mm$$

Segmented Die Design

For the segmented die, the primary factor affecting material failure and signal output level is the cut-away geometry, which is comprised of two factors: the cutting angle (ϕ) and the effective die-wall thickness, see Figure 1a. The primary factors affecting signal linearity are tablet height and position within the die and strain gage arrangement.

Cutting Angle and Die Wall Thickness

For the FEA of cutting angle and die-wall thickness, the model consisted of 144 3-D, 8-nodal solid elements, and 259 nodal points. Because of symmetry, only one-eighth of the segmented die was modeled; this smaller model reduces computation time. An internal die-wall pressure of 120 MPa uniformly applied to the entire inner surface of the die was used to simulate the severest loading conditions. The finite element model was set up with cutting angles of 30°, 60°, 90° and 120°, and with effective die-wall thicknesses of 1, 2, 3, 4, and 5 mm in the cut-away section. The following dimensions were used for all calculations in this section: die bore radius 5.65 mm, external radius 15 mm and die height 25 mm.

The FEA program calculates the Von Mises stress for every nodal point of the segmented die model. The results show that the greatest Von Mises stress occurs on the inner die wall surface while the lowest Von Mises stress occurs in the thickened portion of the outer die wall, and these maximum and minimum Von Mises stresses always occur at these points for all cutting angles and die wall thicknesses examined. One concern in the analysis of failure is the concentration of stress in the corners at edges of the cut-away section. However, calculations clearly show that the Von Mises stress at these outer nodes is well below the Von Mises stress at the inner die wall. Therefore, when analyzing material failure for this segmented die model, stress concentration in these regions can be ignored, because the inner die wall will fail first.

A summary of the FEA results is shown in Figure 2a, where the maximum Von Mises stress, at the inner die wall, is plotted verses the die-wall thickness for each cutting angle. For cutting angles in the range of 30°–120° the maximum Von Mises stress does not change very much; however, increasing the die-wall thickness from 1 to 5 mm decreases the maximum Von Mises stress by approximately 300%.

Calculations like those shown in Figure 2a are essential for the design of a segmented die because they provide the designer with a systematic guide for selecting die-wall thicknesses and cutting angles which do not yield when peak loads are applied. For example, if the desired segmented die has a cutting angle $\phi = 30°$, a safety factor $SF = 1.1$, and a material yield strength $\sigma_{yd} = 340$ MPa, the minimum die-wall thickness that will not yield at a maximum die-wall pressure of 120 MPa can be determined from Figure 2a. By calculating the maximum effective Von Mises stress from the applied stress (i.e. $\sigma_{app} = 340/1.1 = 309$ MPa, Eqn. 3) the minimum die-wall thickness of 4 mm can be read off of Figure 2a, see position A. This result suggests that die-wall yielding may explain why Huckle and Summers (23) found a hysteresis response in their segmented die with a 3 mm die-wall thickness.

In terms of transducer design, the signal output is typically a linear function of the strain (see Eqn. 6) at the gage site; therefore, this analysis of output signal is based upon the surface strain in the cut-away portion of the die. Using the same finite element model, cutting angles and effective die-wall thicknesses as above, the tangential surface strain in the middle of the cut-away section was also calculated. Figure 2b illustrates that when the die-wall thickness is reduced from 5 to 1 mm the average strain increases by a factor of three or more. Generally, the smaller the cutting angle the larger the strain, and for cutting angles less than 60°, the strain is very sensitive to changes in the cutting angle. For example, if $t = 3$ mm, the strain increases approximately 1.5 times when the cutting angle is reduced from 60° to 30°. Based upon Figure 2b, a segmented die with a die

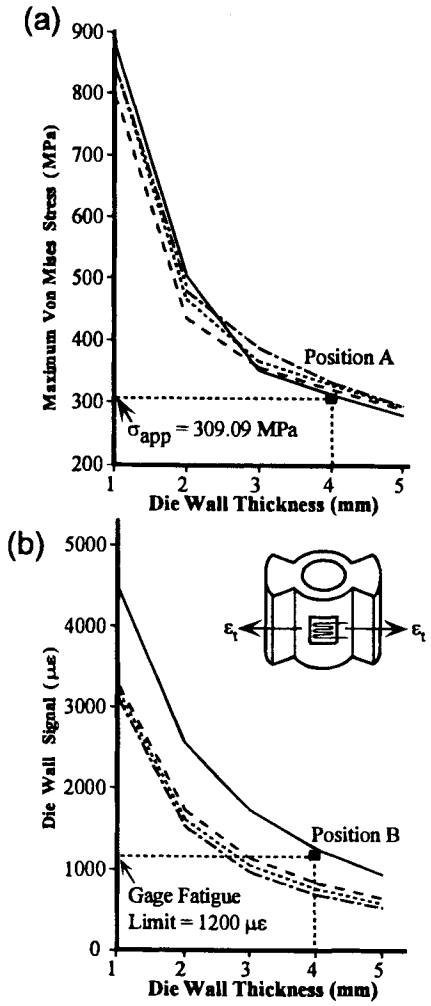

Fig. 2. Maximum Von Mises stress (a) and die wall signal (b) at a 120 MPa die-wall pressure, for four cut-away angles (ϕ = 30°:—, 60°:---, 90°:···, 120°:-·-·) and effective die-wall thicknesses between 1 and 5 mm.

wall thickness of 4 to 5 mm and cutting angles between 60° and 120° will produce an adequate signal.

Also when selecting the optimal dimensions of a segmented die the designer should consider strain gage fatigue limits. For example, if a strain gage with a fatigue limit of 1200 $\mu\varepsilon$ is used on a die with an effective die-wall thickness of 4 mm based upon Figure 2b the cutting angle should be approximately greater than 37°, location B in Figure 2b, in order to prevent strain gage failure.

Tablet Height and Position and Strain Gage Arrangement

By using FEA to reproduce the experimental output signals of Hölzer and Sjögren (7), the effects of tablet height and position and strain gage arrangement on signal linearity can be judged.

The finite element model for the segmented die of Hölzer and Sjögren (7), consisted of 825 3-D, 8-nodal solid elements, and 1196 nodal points, see Figure 3. Because of symmetry, only one-quarter of the segmented die was modeled. To simulate the loading conditions during compaction, the inner die-wall pressure is applied only to the areas where the tablet actually comes in contact with the die wall (see pressure arrows in Figure 3). Consistent with Hölzer and Sjögren's (7) experimental setup, the tablet height (i.e. area in contact with the die wall) was modeled by fixing the upper punch penetration at 4 mm, while the lower punch penetration was varied from 6 to 14 mm in 1 mm increments, and the following parameters were used: die wall thickness 5 mm, cutting angle 30°, bore radius 5.65 mm, external radius 15 mm, die height 25 mm and a constant compaction pressure of 120 MPa. Bridge configuration A had a radial gage at 7 mm and an axial gage at 13 mm while bridge configuration B had a radial gage at 10 mm and an axial gage at 13 mm, below die top.

Based upon the FEA, the Von Mises stress contour and the simulated deformed shape are shown in Figures 4a and 4b, respectively. It should note that Figure 4b is an exaggerated view drawn to better visualize the die-wall deformation, which is actually less than 5 μm. As before, the analysis of signal output is based upon the effective strain Eqn. 7 rather than upon the actual output voltage. The effective strains for bridge configurations A and B are given by $\varepsilon_{eff} = \varepsilon_a - \varepsilon_c$ and $\varepsilon_{eff} = \varepsilon_b - \varepsilon_c$, respectively. Where ε_a and ε_b are the axial strains for the active gages in bridge configurations A and B, respectively, ε_c is the axial strain in the temperature compensating gage.

The effective strain calculated from the data shown in Figure 4b is plotted in Figure 5. This data shows that changing the strain gage location will change signal output, and that for a fixed pressure changes in tablet height will also change signal output. This inherent geometric nonlinearity of the segmented die can be better understood by looking at the Von Mises stress contour. In Figure 4a, the stress contours radiate out in a circular fashion from the area of contact between the die wall and tablet. As a result, the surface strain on the outer die wall varies with location; therefore, signal output will also vary with strain gage location. In addition, because the stress contours radiate out

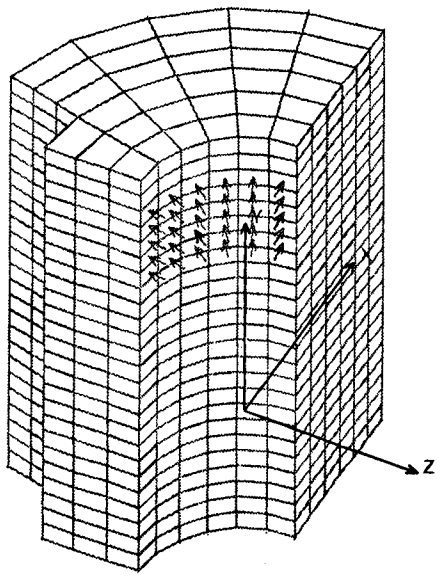

Fig. 3. Finite element model for the tablet-compaction simulation using symmetric segmented die with ϕ = 30°, t = 5 mm and bore radius equal to 11.2 mm. Compact height corresponding to 4 mm upper and 9 mm lower punch penetration and a die-wall pressure equal to 120 MPa shown by arrows.

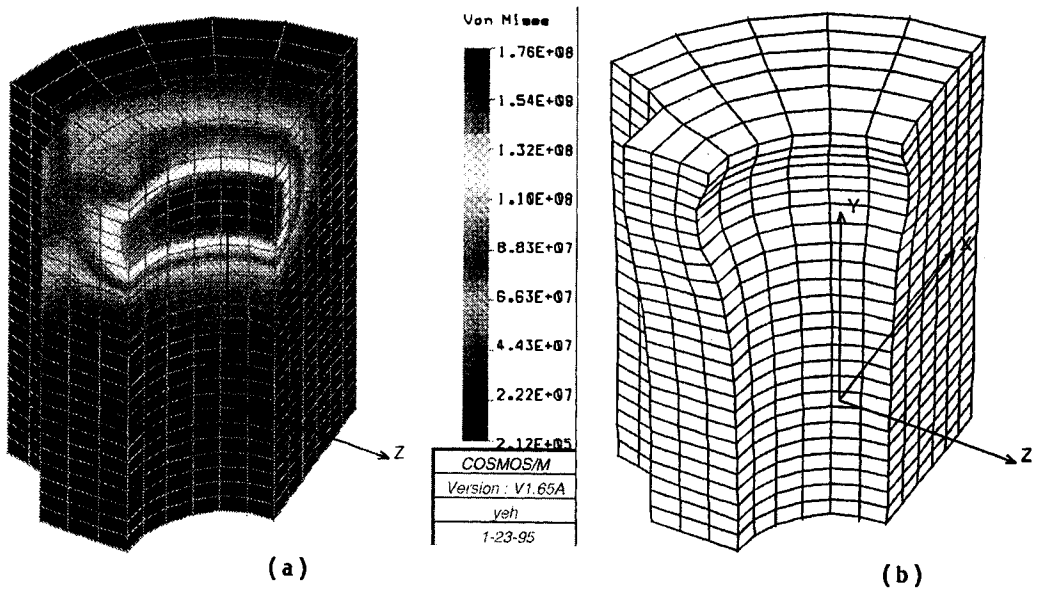

Fig. 4. Tablet-compaction simulation using symmetric segmented die with $\phi = 30°$, $t = 5$ mm and bore radius equal to 11.2 mm. Compact height corresponding to 4 mm upper and 9 mm lower punch penetration and a die-wall pressure equal to 120 MPa, (a) Von Mises stress contour (b) deformed shape.

from the area of contact between the tablet and die wall, the stress distribution (for a fixed pressure) at the outer die wall will also change when the area of contact between the tablet and die wall changes; therefore, signal output will also change when the height of the tablet changes. These results help to explain the well known but often under appreciated fact that the output signal for a segmented die with a fixed tablet height is linear, but when the tablet height and position is varied (as in tablet compaction) the output becomes nonlinear, see Figure 5.

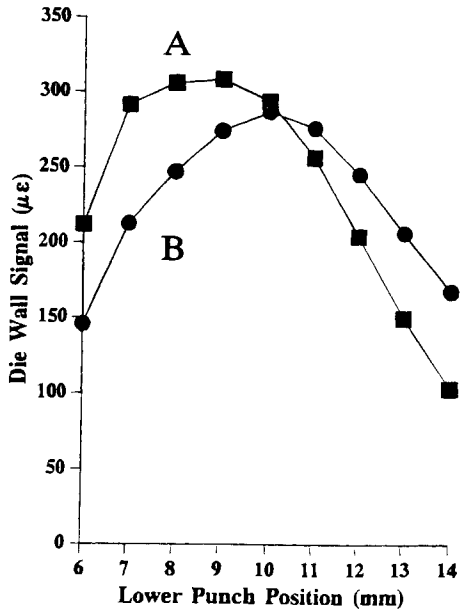

Fig. 5. Calculated die wall signals for different lower punch positions and with a constant upper punch penetration (4 mm); bridge A: ■, bridge B: ●.

These FEA results are in excellent agreement with Hölzer and Sjögren's experimental data. The differences can be explained by errors in estimating parameters such as material properties, compaction pressure and segmented die dimensions. Given these uncertainties, the results are certainly reasonable, and support the validity of the FEA calculations.

Split-Web Design Optimization

Having developed the split-web design concept, the next step is to optimize web thickness and strain gage position according to ODP algorithm.

Web Thickness

Using a uniform inner die wall pressure of 120 MPa to simulate peak loading conditions, the Von Mises stress distribution was calculated. The finite element model uses a total of 630 PLAND2D 4-node, iso-parametric elements, interconnected at 732 nodal points. All the nodal points along the alignment pin holes were restricted in translation but free in rotation. Since the web thickness is small in comparison to the other dimensions and no axial loads are applied, the assumption of plane stress was employed. For the same reasons given previously the die-wall friction was neglected in the FEA calculations.

The greatest Von Mises stress occurs at the inner sensing web arch, while the lowest Von Mises stress occurs in the area around the alignment-pin holes, see Figures 6a and 6b. It should be noted that even though there are two corners, at the base of the sensing-web arch, where the concentration of stress could affect structural integrity the Von Mises stress in these outer regions is still well below the global maximum Von Mises stress on the inner sensing web arch, and thus are not important to this analysis of material failure. In addition, when a prototype is actually made these corners are rounded which further lowers

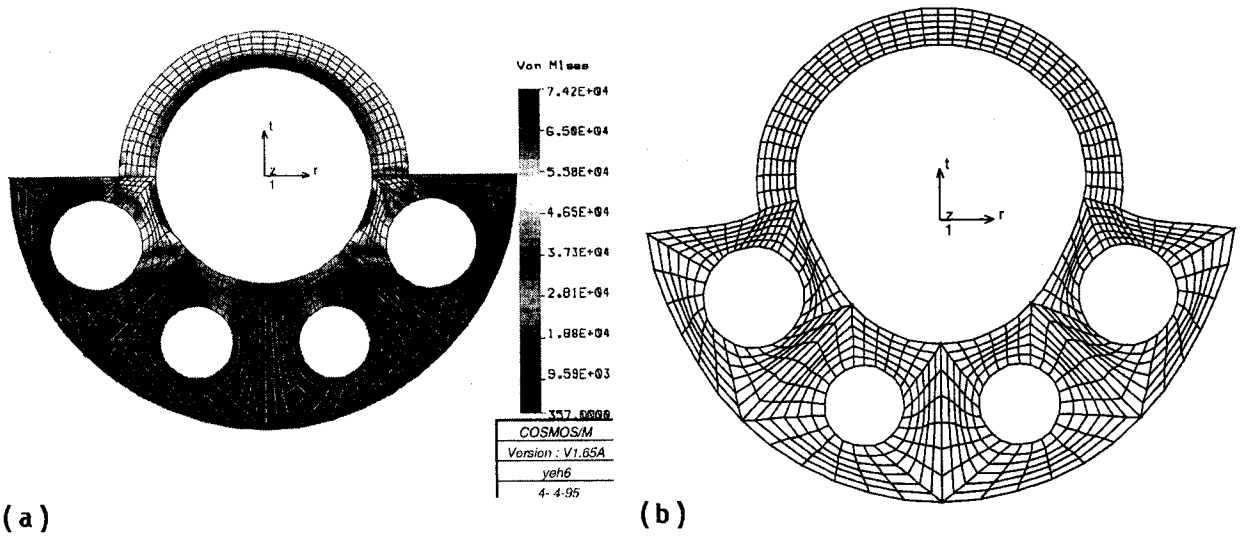

Fig. 6. Von Mises stress contour for the 1/16 in. prototype sensing web at a maximum inner die wall pressure of 120 MPa (a). A deformed 1/8 in. sensing web showing the maximum node displacement at the sensing web arch (b).

the Von Mises stress making the likelihood of the initial material failure occurring in these regions improbable.

As expected, the maximum Von Mises stress decreases as the die wall thickness increases. Because the maximum Von Mises stress of 7.24×10^4 psi in the 1/16 in. sensing web exceeds the material yield strength of 6.4×10^4 psi, the Von Mises failure criterion predicts that failure will occur in the 1/16 in. web but not in the 1/8 in. web, which has a maximum Von Mises stress of 4.96×10^4 psi. To test these predictions, tablets were compacted using the 1/16 and 1/8 in prototype webs. The 1/16 in. sensing web failed at an inner die wall pressure of 120 MPa, while the 1/8 in. sensing web was used many times at this pressure without failing. When the failed 1/16 in. web was examined the permanent deformation occurred in the sensing web arch and not at the corners where stress concentration occurs, thus confirming the accuracy of FEA predictions.

To determine if the strain at the gage site is sufficient to produce a measurable signal, the tangential strain on the outer surface of the sensing web was calculated and compared to the minimum detection limit. Using the same finite element model, the tangential strain for the 1/16 and 1/8 in. sensing web prototypes were calculated from the node displacement. An exaggerated view of the deformed sensing web with an inner die wall pressure of 120 MPa is shown in Figure 6b. As expected the greatest node displacement occurs at the sensing web arch. Note that the actual displacement of the sensing web arch is less than 0.0001 in.

The tangential strains calculated from the node displacement, can be plotted versus angle (ϕ) along the mounting surfaces of sensing web (0° to 90°, see Figure 7). The ε_θ for the 1/16 and 1/8 in. webs varies from 810 to 1091 $\mu\varepsilon$ and from 389 to 508 $\mu\varepsilon$, respectively. These peak strain levels are detectable by most data acquisitions systems. Therefore, the authors recommend a web thickness of 1/8 in., which has a built in safety factor of approximately 15%.

Strain Gage Location

Strain gage position on the sensing web is also a critical design factor, because a strain gage that is placed in an area of high stress concentration (high strain gradient) may produce inaccurate results. This can occur because strain gages average the strain over the area covered by the grid, improper averaging of strain may occur in areas with steep strain gradients. Figure 7 shows the relationship between outer die-wall strain and strain gage position on the sensing web. The strain gradient (slope of strain vs. ϕ) is smallest at $\phi = 0°$, and highest at $\phi = 90°$ (i.e. around the edges of sensing web). Therefore, the authors recommend placing a single strain gage at $\phi = 0°$ or placing two strain gages at $\phi = \pm 30°$.

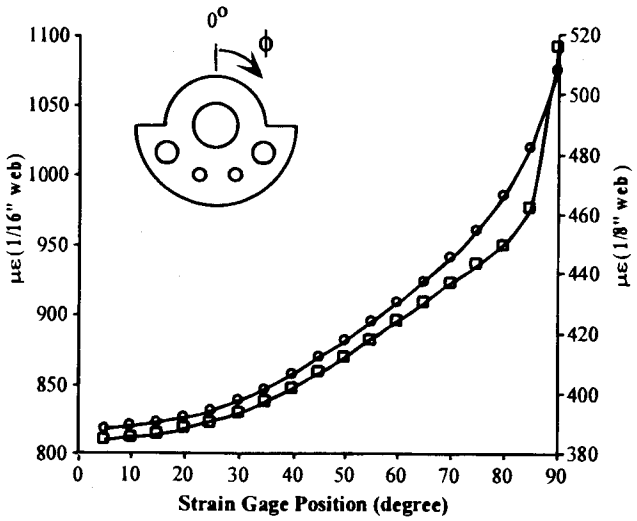

Fig. 7. Effect of web thickness and strain gage location on the tangential strain for the 1/8: ○ and 1/16: □ in. sensing webs. The sensing web drawn within the figure shows the position of the zero degree angle mark.

Signal Linearity

To theoretically verify output signal linearity, a strain calibration curve was calculated for strain gages on the 1/8 in. sensing web positioned at $\phi = 0°$, 30° and 60°, and with

inner die wall pressures ranging from 0 to 120 MPa. A linear relationship was observed for all the three strain gage positions.

Die Calibration

The experimental calibration curve for the 1/8 in. split-web die was linear with a 99.9% correlation. Note with this method of calibration, the application of pressure caused the height of the neoprene calibration tablet to change from almost 7/8 in. to 3/8 in.. The linear signal illustrates an advantage of layered dies over other transducer types. In addition, hysteresis phenomenon can be used to judge transducer performance (13). Hysteresis is defined as a deviation from linearity in which the unloading curve falls below the loading curve, and when seen, indicates material or strain gage yielding. When signal output from the instrumented die was measured for both loading and unloading, no hysteresis was observed, thereby substantiating both the Von Mises strength and the signal output calculations. Lack of hysteresis also indicates that the neoprene used for calibration doesn't affect the calibration results (8).

Evaluation of Optimized Design

To test the performance of the transducer designed by using ODP, the compaction characteristics of some well characterized excipients were studied using radial versus axial stress transmission curves (pressure-cycle curves). Figures 8a and 8b show representative pressure-cycle curves for NaCl and starch 1500, respectively. Despite some differences these results are in general agreement with the literature (24,25), which helps to validate the transducer design. Also, it is interesting to note that the slope of the pressure-cycle curve for starch shifts downward when the die wall was not lubricated prior to tablet compaction, indicating that different compaction conditions can be observed with the split-web die.

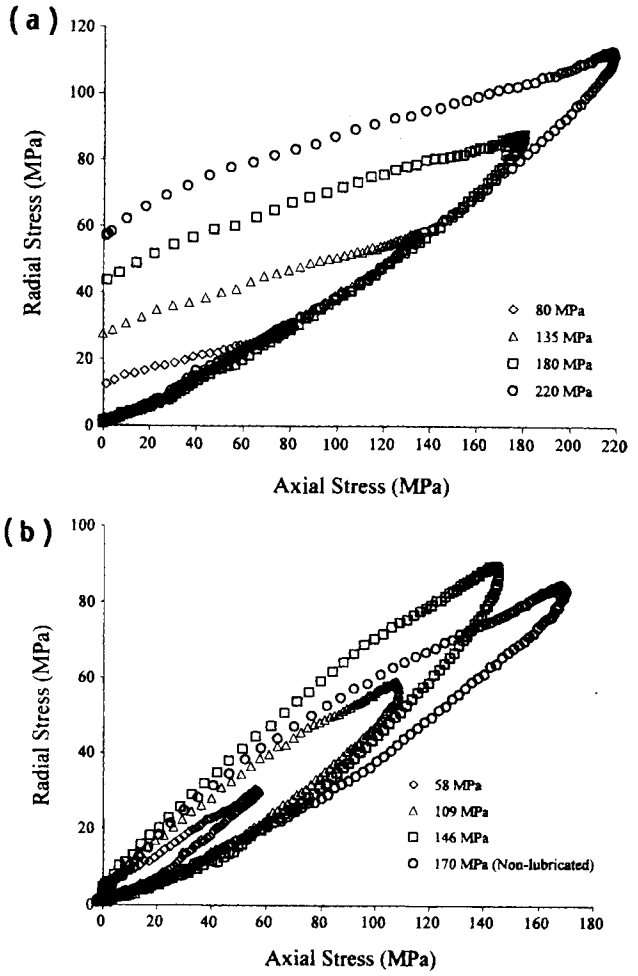

Fig. 8. Radial versus axial stress transmission curves for sodium chloride (a) and Starch 1500 (b) using 1/8 in. sensing web. Legend indicates peak axial pressures.

CONCLUSIONS

Based upon engineering stress analysis, this study presents a general methodology for designing tablet press instrumentation. The ODP coupled with FEA and the power of personal computers enables the designer to simulate design performance for a wider range of loading conditions, strain gage arrangements, and design configurations than would be possible with the trial-and-error design methods, which reduces design time, cost, and improves performance and reliability. In addition, because transducers for die-wall stress measurement can produce ambiguous results, the improved theoretical understanding gained through the design-by-analysis approach will help researchers better interpret data and better understand the data's limitations.

The split-web die concept developed by the authors, encloses the sensing web in a cylinder, thereby allowing the instrumented die to be mounted without modification of the die table. This design overcomes a limitation with three-layered die transducer and thus improves DWS measurement. The optimal web thickness and strain gage position were determined using the optimal design process. Based upon FEA, the authors recommend the use of the 1/8 in. sensing web and a strain gage positioned at $\phi = 0°$, or two gages at $\phi = \pm 30°$, for optimal signal output. This system showed no hysteresis, which indicates that there is no permanent distortion of the 1/8 in. sensing web in the range of pressures studied.

ACKNOWLEDGMENTS

This research forms part of the doctoral thesis submitted by Syed A. Altaf to the Graduate School at Oregon State University. The authors wish to thank the Eli Lilly and Company and AACP Young Investigators Grant for its generous financial support and Carol A. Roberts for her typing of the manuscript.

REFERENCES

1. E. Nelson. *J. Am. Pharm. Assn. Sci. Ed* **44**:494–497 (1955).
2. J. J. Windheuser, J. Misra, S. P. Eriksen, and T. Higuchi. *J. Am. Pharm. Assn.* **52**:767–772 (1963).
3. K. Ridgway and P. H. Rosser. *J. Pharm. Pharmacol.* **23**:202S–209S (1971).
4. U. Conte, P. Colombo, A. L. Manna, and C. Caramella. *Il Farmaco—Ed. Pr.* **32**:551–559 (1977).
5. Y. Kanaya, T. Ando, and K. Asahina. *Yakuzaigaku* **39**:26–33 (1979).
6. E. G. Rippie and D. W. Danielson. *J. Pharm. Sci.* **70**:476–482 (1981).
7. A. W. Hölzer and J. Sjögren. *Int. J. Pharm.* **3**:221–230 (1979).
8. P. D. Huckle and M. P. Summers. *J. Pharm. Pharmacol.* **37**:722–725 (1985).
9. H. G. Cocolas and N. G. Lordi. *Drug. Dev. Ind. Pharm.* **19**:2473–2497 (1993).

10. S. Timoshenko and J. N. Goodier. *Theory of Elasticity*, McGraw-Hill, New York, 1970.
11. J. A. Collins. *Failure of Materials in Mechanical Design: Analysis, Prediction, Prevention*, John Wiley & Sons, New York, 1993.
12. D. G. Ullman. *The Mechanical Design Process*, McGraw-Hill, New York, 1992.
13. J. W. Dally and W. F. Riley. *Experimental Stress Analysis*, McGraw-Hill, New York, 1978.
14. A. L. Window. *Strain Gauge Technology*, Elsevier Science Publishers Ltd., Amsterdam, 1992.
15. R. D. Cook. *Concepts and Applications of Finite Element Analysis*, John Wiley & Sons, New York, 1981.
16. S. S. Rao. *The Finite Element Method in Engineering*, Pergamon Press, Oxford, 1982.
17. E. R. Champion, *in* "Finite element analysis in manufacturing engineering: A PC-based approach", p. 31–66. McGraw-Hill Inc., New York, 1992.
18. P. R. Watt. *Tablet Machine Instrumentation in Pharmaceutics: Principles and Practice*, Ellis Horwood Limited, New York, 1988.
19. E. Nelson, S. M. Naqvi, L. W. Busse, and T. Higuchi. *J. Am. Pharm. Assn.* **43**:596–602 (1954).
20. W. A. Strickland, T. Higuchi, and L. W. Busse. *J. Am. Pharm. Assn.* **49**:35–40 (1960).
21. A. M. Salpekar and L. L. Augsburger. *J. Pharm. Sci.* **63**:289–293 (1974).
22. R. T. Fenner. *Engineering Elasticity*, Ellis Horwood, Chichester, England, 1986.
23. P. D. Huckle and M. P. Summers. *J. Pharm. Pharmacol* **36**:Suppl. 6P (1984).
24. S. Leigh, J. E. Carless, and B. W. Burt. *J. Pharm. Sci.* **56**:888–892 (1967).
25. E. Shotton and B. A. Obiorah. *J. Pharm. Pharmacol.* **25**:Suppl.:37–43 (1973).